


## Prethermalization in aperiodically kicked many-body dynamics

Jin Yan<sup>1,2</sup>, Roderich Moessner<sup>1</sup>, and Hongzheng Zhao<sup>1,3,\*</sup>

<sup>1</sup>Max Planck Institute for the Physics of Complex Systems, Nöthnitzer Straße 38, 01187 Dresden, Germany

<sup>2</sup>Weierstrass Institute for Applied Analysis and Stochastics, Mohrenstraße 39, 10117, Berlin, Germany

<sup>3</sup>School of Physics, Peking University, 100871 Beijing, China

 (Received 4 July 2023; revised 15 January 2024; accepted 17 January 2024; published 13 February 2024)

Driven many-body systems typically experience heating due to the lack of energy conservation. Heating may be suppressed for time-periodic drives, but little is known for less regular drive protocols. In this paper, we investigate the heating dynamics in aperiodically kicked systems, specifically those driven by quasiperiodic Thue-Morse or a family of *random* sequences with  $n$ -multipolar temporal correlations. We demonstrate that multiple heating channels can be eliminated *even away from the high-frequency regime*. The number of eliminated channels increases with multipolar order  $n$ . We illustrate this in a classical kicked rotor chain where we find a long-lived prethermal regime. When the static Hamiltonian only involves the kinetic energy, the prethermal lifetime  $t^*$  can strongly depend on the temporal correlations of the drive, with a power-law dependence on the *kick strength*  $t^* \sim K^{-2n}$ , for which we can account using a simple linearization argument.

DOI: [10.1103/PhysRevB.109.064305](https://doi.org/10.1103/PhysRevB.109.064305)

### I. INTRODUCTION

Time-dependent many-body systems have attracted sustained interest due to their ubiquity in nature and the potential to realize nonequilibrium phases of matter. One typical example is the discrete time crystal which spontaneously breaks discrete time translation symmetry (TTS) [1,2]. However, due to the absence of energy conservation, closed driven systems tend to heat up and lose any nontrivial correlations [3,4]. Therefore, understanding and controlling the onset of heating in time-dependent systems is key to their stabilization and to the realization of exotic nonequilibrium phenomena.

While heating generally occurs in time-dependent many-body systems, it can be parametrically suppressed, e.g., by using high-frequency drives [5–14] or by using weak drive amplitudes [15–17] in periodically driven (Floquet) systems. Examples include spin systems with a bounded local energy scale, where an exponentially long-lived prethermal regime appears before heating takes over [15,18–24]. A similar prethermal phenomenon can also manifest in kicked systems which have been extensively studied in the context of digital quantum simulation [9,25,26] and the fundamental discussion of chaos [27–32]. A paradigmatic example is the interacting kicked rotor, where heating takes the form of Arnold diffusion [33–42]: Before their eventual diffusive dynamics with unbounded energy growth [29], heating only occurs with a

probability exponentially small in the kick strength in the prethermal regime [43].

It is natural to ask: Can heating be efficiently suppressed in many-body systems without TTS, e.g., when drives are quasiperiodic or even random? This is a notoriously difficult question, as breaking TTS generally opens up further deleterious heating channels that can destabilize systems rapidly [44–46]. For certain piecewise constant and continuous quasiperiodic drives, this is known to be possible in the high-frequency regime [47–58]. Rigorous bounds on heating rates can also be established by generalizing the Floquet theory [59,60]. However, this becomes obscure for kicked systems as the high-frequency limit of kicks in principle allows a divergent rate of energy input into the system. Aperiodically kicked systems have been most limited to few-body settings [61–65], and it remains an outstanding challenge to control heating in the thermodynamic limit.

Here, we give an affirmative answer by investigating many-body systems kicked by a family of structured binary random protocols—random multipolar drives (RMDs) [51]. They exhibit a multipolar correlation indexed by an integer  $n$ : for  $n = 0$ , the drive is purely random and generated from binary options  $\{s_0^+, s_0^-\} = \{+, -\}$ ; for  $n = 1$ , it consists of a random sequence of two elementary dipolar blocks,  $\{s_1^+, s_1^-\} = \{(-, +), (+, -)\}$ ; and the  $n$ th.-order multipolar blocks are recursively generated by concatenating two different  $(n-1)$ th.-order blocks,  $\{s_n^+, s_n^-\} = \{(s_{n-1}^-, s_{n-1}^+), (s_{n-1}^+, s_{n-1}^-)\}$ . In the  $n \rightarrow \infty$  limit,  $s_n^\pm$  produces the quasiperiodic Thue-Morse (TM) sequence [60,66]. An RMD notably suppresses low-frequency components in the driving spectrum, reducing heating algebraically in the high-frequency regime [51].

In this paper, instead of focusing on the high-frequency regime, we exploit the self-similarity inherent in the RMD sequence to demonstrate that heating can be parametrically controlled by the kick strength. Through a perturbative

\*hzhao@pks.mpg.de

Published by the American Physical Society under the terms of the [Creative Commons Attribution 4.0 International license](https://creativecommons.org/licenses/by/4.0/). Further distribution of this work must maintain attribution to the author(s) and the published article's title, journal citation, and DOI. Open access publication funded by the Max Planck Society.

expansion, we derive an effective Hamiltonian governing the initial time evolution. Remarkably, the self-similar multipolar structure leads to exact cancellations of numerous terms in the effective Hamiltonian, thereby eliminating the corresponding heating channels. This mechanism of heating suppression is independent of the specific model and is applicable to both quantum and classical many-body systems.

For numerical efficiency, we demonstrate this effect in a concrete model, namely, a kicked chain of classical rotors. Starting from low-temperature initial states, the system exhibits a long-lived prethermal regime before heating up. The lifetime scaling depends on the microscopic details of the kicked system, and if the static part only involves the kinetic energy, the lifetime scales as a power law with a tunable exponent  $2n$ . This we account for by analyzing the linear stability of the system. In the quasiperiodic TM limit, we also show that the lifetime grows faster than any power law but slower than exponentially.

In the following, we first consider a general kicked system and demonstrate heating suppression in a perturbative expansion of the effective Hamiltonian in the small kick strength. We then present the results on the chain of rotors before a concluding discussion.

## II. SETTING

Consider the time-dependent Hamiltonian  $H(t) = H + V\Delta(t)$ , where  $H$  denotes the static part, and  $V$  defines the kick with  $\Delta(t) = \sum_l K_l \delta(t - l\tau)$ , with the kick strength  $K_l$  and period  $\tau$ . We focus on the intermediate frequency regime, i.e.,  $\tau$  is not necessarily small. Here,  $K_l$  is binary ( $\pm K$ ) and follows an  $n$ -RMD sequence. For  $n = 0$ , there are two unitary time evolution operators  $U_0^\pm = e^{-i\tau H} e^{\mp iKV}$ . We can formally define the static effective Hamiltonian  $H_0^\pm$  through the relation  $U_0^\pm = \exp(-i\tau H_0^\pm)$  to describe the dynamics at times  $t = l\tau$ . For small  $K$ , this Hamiltonian can perturbatively constructed as  $H_0^\pm = \sum_{m=0}^{\infty} K^m \Omega_{0,m}^\pm$ . Although such an expansion may diverge for many-body systems, we expect its truncation at low orders in  $K$  can approximate the initial time evolution. The lowest-order term is simply the static Hamiltonian  $\Omega_{0,0}^\pm = H$ .

Via the replica resummation of the Baker-Campbell-Hausdorff series, the leading correction can be expressed in a compact form [15]:

$$\Omega_{0,1}^+ = -\Omega_{0,1}^- := \Omega_{0,1} = \frac{-i\text{ad}_H \exp(-i\tau \text{ad}_H)}{\exp(-i\tau \text{ad}_H) - 1} V, \quad (1)$$

where  $\text{ad}_X(Y) = [X, Y]$  is the Lie derivative. It can also be expanded in a power series in  $\tau$  as

$$\Omega_{0,1} = V\tau^{-1} - \frac{i[H, V]}{2} + O(\tau^1), \quad (2)$$

where higher-order terms only contain nested commutators of the form  $[H, V]_s := [H, \dots, [H, V] \dots]$  with a single kick  $V$  but multiple ( $s$ )  $H$  operators. Note, since  $\tau$  is not necessarily small, one should consider all orders in  $\tau$  in the expansion. Generally,  $\Omega_{0,1}$  does not vanish, and the time evolution is dominated by  $H \pm K\Omega_{0,1}$  initially. The term  $\Omega_{0,1}$  occurs randomly with an amplitude linear in  $K$ , and one expects it to quickly destabilize the system and induce heating in a short time.

We now use the self-similar structure of RMD protocols to show that many terms of order  $O(K)$  in the effective Hamiltonian can be eliminated. Further, if the condition

$$[H, V]_s = 0 \quad (3)$$

can be satisfied for  $\forall s \geq n_c$  with some integer  $n_c$ , for  $n$ -RMD systems with any  $n \geq n_c$ , random perturbations start appearing at a higher order  $O(K^3)$ , and hence, heating can be significantly suppressed.

To see this, we first observe that higher-order multipolar operators can be obtained by the recursive relation:

$$U_n^\pm = U_{n-1}^\mp U_{n-1}^\pm, \quad (4)$$

where  $U_n^\pm$  generates the time evolution over the duration  $2^n\tau$  [51]. For  $n$ -RMD systems, the time evolution is given by a random sequence of multipolar operators  $U_n^\pm$ . Similarly, the effective Hamiltonian  $H_n^\pm$  is defined through  $U_n^\pm = \exp(-i2^n\tau H_n^\pm)$ , governing the stroboscopic time evolution ( $t = 2^n\tau l$  for integers  $l$ ). The perturbative expansion is denoted as  $H_n^\pm = \sum_{m=0}^{\infty} K^m \Omega_{n,m}^\pm$ . Notably, the time evolution operators in  $U_0^\pm$  possess the special property that  $U_0^+$  can be mapped to  $U_0^-$  by changing  $K \rightarrow -K$ . Thus, terms in the effective Hamiltonians coincide for even orders in  $K$ , while differing by a minus sign for odd orders, given by

$$\Omega_{n,m}^+ = (-1)^m \Omega_{n,m}^- := \Omega_{n,m}. \quad (5)$$

Like the purely random drive ( $n = 0$ ), the initial stroboscopic time evolution is governed by  $H \pm K\Omega_{n,1}$ , and the system may still exhibit rapid heating. However, the self-similar construction in Eq. (4) and the symmetry property in Eq. (5) lead to an important result: Several terms in  $\Omega_{n,1}$  actually vanish, resulting in

$$\Omega_{n,1} = \sum_{s=n}^{\infty} f_{n,s} \tau^s [H, \Omega_{0,1}]_s, \quad (6)$$

where the coefficient  $f_{n,s}$  can be cumbersome to obtain. Importantly, it suggests that, to the leading order of  $O(K)$ , the only possible heating channels are in the form of  $[H, V]_s$  with  $s \geq n$ . The derivation of Eq. (6) is presented in Appendix A. Now if the condition Eq. (3) is satisfied, all terms in  $\Omega_{n,1}$  vanish. Consequently, the stroboscopic time evolution of the system is effectively governed by  $H_n^\pm = \bar{H}_n \pm O(K^3)$ , where the static part is denoted by  $\bar{H}_n = H + K^2\Omega_{n,2}$ . Therefore, the RMD kicked systems first relax to a prethermal ensemble determined by  $\bar{H}_n$  before notable heating is induced by random perturbations of order  $O(K^3)$ .

Although we use the perturbative expansion for quantum systems, it is important to note that this mechanism of heating suppression equally applies to classical many-body systems. The Liouville equation, which describes the phase-space distribution of a classical system, exhibits a structural similarity to the Schrödinger equation in quantum systems. Consequently, the effective Hamiltonian for classical systems can be obtained by formally replacing the commutator  $[\dots]/i$  in its quantum counterpart with the Poisson bracket  $\{\dots\}$  [18]. Due to the computational efficiency of numerical simulations for large classical systems, we proceed to demonstrate this heating suppression in a classical rotor system.

### III. MANY-BODY KICKED ROTORS

We consider many-body rotors with the static kinetic energy ( $H = H_{\text{kin}}$ ) and the kicked nearest-neighboring interactions ( $V = V_{\text{int}}$ ):

$$H_{\text{kin}} = \frac{1}{2} \sum_j \frac{p_j^2}{M}, \quad V_{\text{int}} = \sum_j \cos(q_{j+1} - q_j), \quad (7)$$

where  $M$  denotes the angular mass. We consider the regime  $\tau/M \gg K$ , and for simplicity, we set  $M = 1$  and  $\tau = 1$ . Here,  $p_j$  and  $q_j$  for  $j = 1, \dots, N$  are the conjugate angular momenta and angles of  $N$  rotors, respectively. Periodic boundary conditions are used ( $q_1 = q_{N+1}$ ). The interaction preserves the total angular momentum  $\sum_{j=1}^N p_j$ . The kicked rotor system is different from the popular step-wise driven spin models in two ways: First, kicks can allow a divergent energy input in the high-frequency regime; second, rotors have unbounded kinetic energy, hence permitting an unbounded energy absorption from the kicks. In Appendix B, we numerically demonstrate that the system can heat up increasingly fast when  $\tau$  becomes smaller. In the following, we will show that, despite this potential instability of kicked rotors, heating can be parametrically suppressed away from the high-frequency limit by exploiting the self-similar structure of the drive.

As we will demonstrate, Eq. (3) can be approximately satisfied with a narrow angular momentum distribution. In the prethermal regime, the distribution width is determined by the controllably small temperature  $T \sim K^2$ .

To begin, we derive the nested Poisson brackets  $\{H, V\}_s$  for kicked rotors, which reduce to  $\sum_j (p_j - p_{j+1})^s \sin(q_j - q_{j+1})$  for odd  $s$  and  $\sum_j (p_j - p_{j+1})^s \cos(q_j - q_{j+1})$  for even  $s$ . Thus, for multipolar order  $n \geq 1$ , Eq. (6) implies that the dominant random perturbation  $\Omega_{n,1}$  only contains terms proportional to  $(p_j - p_{j+1})$  or its higher powers. These terms become negligible when the kinetic energy distribution is sufficiently narrow. For higher multipolar orders  $n$ , Eq. (3) can be more effectively satisfied, and thus, the suppression becomes stronger.

When starting from the initial condition  $p_j = \tilde{p}$  for all  $j$ , Eq. (3) is fulfilled exactly, and the initial time evolution is governed by the static effective Hamiltonian  $\tilde{H}_n = H_{\text{kin}} + K^2 \Omega_{n,2}$ . As this Hamiltonian is generally nonintegrable, the angular momentum distribution spreads. In the prethermal regime, it approximately reaches the Gibbs distribution  $\prod_{j=1}^N \exp[-(p_j - \tilde{p})^2 / 2T]$  [43]. The width of the distribution is determined by an effective prethermal temperature  $T$ . As shown in Appendix C, this temperature is controllably small for weak kicks ( $T \sim K^2$ ).

### IV. NUMERICAL SIMULATION

We now confirm the possibility of prethermalization through numerical simulations. The stroboscopic time evolution of RMD kicked rotors can be generated by a set of discretized equations of motion (EOMs):

$$p_j(t+1) = p_j(t) \pm K \{ \sin[q_{j+1}(t) - q_j(t)] + \sin[q_{j-1}(t) - q_j(t)] \}, \quad (8)$$

$$q_j(t+1) = q_j(t) + \tau p_j(t+1), \quad (9)$$

for  $j = 1, 2, \dots, N$ ,

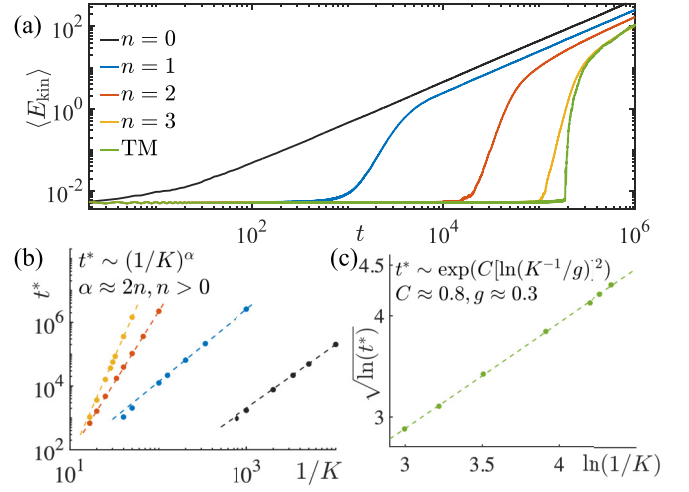


FIG. 1. (a) Time evolution of the averaged kinetic energy for  $n$ -random multipolar drive (RMD) and Thue-Morse (TM) drive with  $K = 0.03$  in a log-log scale. (b) Dependence of the prethermal lifetime  $t^*$  on  $1/K$  in a log-log scale. Dashed lines ( $K^{-2n}$  for  $n > 0$  and  $K^{-2}$  for  $n = 0$ ) are plotted to guide the eyes. (c) Prethermal lifetime  $t^*$  scaling for TM drives.

where  $\pm$  follows the RMD sequence, and  $t$  labels the number of kicks. We choose  $\tau = 1$  and use a small kick strength  $K$  in the following.

The spreading of the angular momentum distribution can be quantified by the kinetic energy density  $E_{\text{kin}}(t) := \frac{1}{2N} \sum_{i=1}^N p_i^2(t)$ , making it a suitable measure of the heating process. The initial conditions are chosen as  $q_j \sim \text{Uni}[0, 2\pi]$ , and  $p_j = 0.1$  is fixed for all  $j$ , satisfying the condition, Eq. (3). Figure 1(a) depicts the dynamics of the averaged kinetic energy  $\langle E_{\text{kin}} \rangle$ , averaged over 350 noise realizations with different initial states, for a fixed kick strength  $K = 0.03$  and rotor number  $N = 500$ . The system size is sufficient to mimic the heating behavior in thermodynamically large systems. Discussions regarding finite-size effects can be found in Appendix I, and the simulation details can be found in Appendix D. For multipolar order  $n \geq 1$ ,  $\langle E_{\text{kin}} \rangle$  remains almost unchanged for a long time scale  $t^*$ . However, as the kinetic energy is unbounded, it eventually increases when heating takes over. This behavior is qualitatively similar to the periodically kicked rotors, cf. Appendix E. We observe that, for larger  $n$ ,  $t^*$  remarkably extends by several orders of magnitude, reaching its largest value in the TM limit. In contrast, for the fully random drive ( $n = 0$ ), unbounded diffusion starts at very early times, and no prethermal regime can be established.

We quantify the prethermal lifetime  $t^*$  and its dependence on  $K$ . We extract  $t^*$  by fitting  $\langle E_{\text{kin}} \rangle$  up to time  $t_f$  with a power law  $t^b$  and monitor the power  $b$  for different  $t_f$  [43]. During the prethermal regime, the power  $b$  remains close to zero, and  $t^*$  is determined when  $b$  first reaches a threshold. In our numerical simulations, we choose  $b = 0.05$ , but our findings are independent of the specific threshold value as long as it is small.

Figure 1(b) illustrates the dependence of  $t^*$  on the kick strength for different multipolar orders. A linear fit in a log-log scale suggests that the prethermal lifetime follows an algebraic dependence on the kick strength  $t^* \sim (1/K)^\alpha$ . The scal-

ing exponent  $\alpha$  can be determined through numerical fitting. For  $n = 0$ ,  $\alpha \approx 2$  and remains approximately the same for  $n = 1$ , although the prefactor differs by three orders of magnitude, indicating significant heating suppression due to the dipolar structure. Interestingly, for higher multipolar orders,  $\alpha$  notably increases and is well approximated to  $\alpha \approx 2n$  for  $n = 1, 2, 3$ . In the TM limit, the lifetime scaling converts to

$$t^* \sim \exp \left\{ C \left[ \ln \left( \frac{K^{-1}}{g} \right) \right]^2 \right\}, \quad (10)$$

where the constant  $C \approx 0.8$  and  $g \approx 0.3$ , as shown in Fig. 1(c). A similar functional form has been rigorously proved in Ref. [60] for high-frequency drives, and it remains an open question to justify such a dependence on  $K$ . We also verify that this scaling grows faster than any power law (cf. Appendix F), indicating a significant suppression of heating in a nonperturbative manner.

## V. LINEARIZATION

Although it is expected that a larger  $n$  may further suppress heating, the perturbative expansion of the effective Hamiltonian is insufficient to explain the prethermal lifetime scaling. To address this, we develop a simple theory by linearizing the many-body systems.

Assuming small angular differences between neighboring rotors  $(q_j - q_{j+1}) \bmod 2\pi \ll 1$ , we can expand the kicked interaction using the quadratic approximation  $\cos(q_j - q_{j+1}) \approx 1 - \frac{1}{2}(q_j - q_{j+1})^2$  in the Hamiltonian Eq. (7). Performing a Fourier transform, we obtain

$$H(t) = \frac{1}{2} \sum_w \left[ |P_w|^2 \pm F(w) |Q_w|^2 \sum_l \delta(t - l\tau) \right], \quad (11)$$

where  $w := 2\pi I/N$  for an integer  $I$ ,  $F(w) := 4K \sin^2(w/2)$ , and the Fourier components are defined as  $P_w = \sum_{j=1}^N p_j e^{-iwj}/\sqrt{N}$  and  $Q_w = \sum_{j=1}^N q_j e^{-iwj}/\sqrt{N}$ . The system now decouples into a set of independent kicked harmonic oscillators labeled by  $w$ . For each oscillator, we can integrate its discrete time evolution in a two-dimensional phase space over one period  $\tau$ :

$$\begin{pmatrix} Q_w \\ P_w \end{pmatrix}_{t+\tau} = M_0^\pm(w) \begin{pmatrix} Q_w \\ P_w \end{pmatrix}_t, \quad (12)$$

where (cf. Appendix G 1)

$$M_0^\pm = \begin{pmatrix} 1 \mp \tau F & \tau \\ \mp F & 1 \end{pmatrix} \quad (13)$$

is the elementary evolution matrix, and we drop the label  $w$ , as the following discussion equally applies to all  $w$ .

Similar to Eq. (4), higher multipolar evolution matrices can be recursively derived as  $M_n^\pm = M_{n-1}^\mp M_{n-1}^\pm$  to generate stroboscopic time evolution over the duration  $2^n \tau$ . Crucially, both  $M_n^+$  and  $M_n^-$  have the property  $\det(M_n^\pm) = 1$ , making them area-preserving maps [67]. Therefore, when only  $M_n^+$  or  $M_n^-$  is periodically applied, the system, for weak kicking strength, exhibits nonchaotic dynamics confined to a closed elliptical orbit around its fixed point  $(Q, P) = (0, 0)$ . However, the random concatenation of two slightly different maps

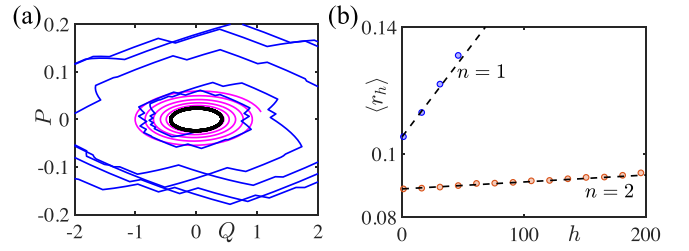


FIG. 2. (a) Trajectories in phase space. The black orbit is obtained by the area-preserving map  $\bar{M}_n$ . The magenta curve with a constant expansion rate is generated via  $\bar{M}_1$ . The blue curve is a single realization obtained by stochastically applying the matrix  $M_1^\pm$ . (b) The averaged radius  $\langle r_h \rangle$  matches well with theoretical predictions (dashed lines).  $F = 0.08$  is used in both panels.

$M_n^\pm$  generally perturbs these stable trajectories, causing them to deviate indefinitely from their fixed points [Fig. 2(a), blue]. By quantifying such deviation, one can estimate the heating rate and its relation to the multipolar order.

To analyze this deviation, we define the averaged evolution matrix as  $\bar{M}_n := \frac{1}{2}(M_n^+ + M_n^-)$  and the difference between the two matrices as  $D_n := \frac{1}{2}(M_n^+ - M_n^-)$ , such that  $M_n^\pm = \bar{M}_n \pm D_n$ . It is worth noting that  $\det(\bar{M}_n) = 1 + O((\tau F)^{2n})$  for nonzero  $n$ , indicating that the averaged map  $\bar{M}_n$  does not preserve area in phase space. Instead, the trajectory slowly spirals out with a constant expansion rate scaling as  $F^{2n}$  [magenta in Fig. 2(a)]. Additionally, eigenvalues of the stochastic term  $D_n$  scale as  $F^n$  (cf. Appendix G 3), which contributes to a diffusive spiral-out process with a rate that also scales as  $F^{2n}$ .

To quantify this process, we introduce the normalized map  $\bar{M}_n' = \bar{M}_n / \sqrt{\det \bar{M}_n}$ , which is now area-preserving and generates a closed elliptical orbit [Fig. 2(a), black]. Its matrix elements define the metric of the orbit and determine its area  $A(Q, P)$  [68]. The radius of the ellipse  $r_h = \sqrt{A(Q, P)/\pi}$  will become time dependent when  $M_n^\pm$  is stochastically applied  $h$  times. The expansion rate of the radius can be calculated as  $\Delta r_h / r_h$ , where  $\Delta r_h = r_{h+1} - r_h$ . By averaging over different random realizations and the polar angle of the ellipse, we find that its leading-order contribution scales as  $F^{2n}$ , with a specific expression  $\langle \Delta r_h / r_h \rangle \approx 3\tau^2 F^2 / 4$  for  $n = 1$  and  $6\tau^4 F^4$  for  $n = 2$ , cf. Appendix G 2. Consequently, the averaged growth of the radius at early times can be obtained.

In Fig. 2(b), we present numerical simulations (circles) of the averaged radius for  $n = 1$  (blue) and 2 (orange), which closely match our analytical predictions (dashed lines). As  $F$  is proportional to the kicking strength, the expansion rate scales as  $K^{2n}$ , and its inverse corresponds to the observed prethermal lifetime scaling in Fig. 1.

Notably, the strong dependence of the multipolar order in the lifetime scaling is remarkably robust, even for initial states that deviate significantly from the linearization regime, where  $(q_j - q_{j+1}) \bmod 2\pi \ll 1$ . Indeed, our numerical results in Fig. 1 are obtained using a random distribution of  $q_j$  over a wide range  $[0, 2\pi]$ . In Appendix H, we confirm that this phenomenon persists as long as the prethermal regime exhibits a low temperature, leading to a narrow distribution of angular momenta.

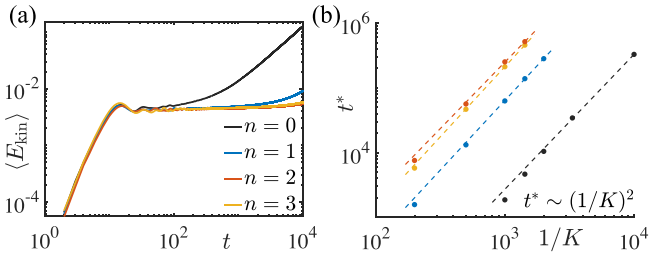


FIG. 3. (a) Time evolution of the averaged kinetic energy density for different multipolar order  $n$  with  $K = 0.005$  in a log-log scale. (b) Prethermal lifetime  $t^*$  as a function of  $1/K$  in a log-log scale. The system starts from the initial angular momentum  $p_j(0) = 0$  with  $B = 0.01$ . Other numerical parameters are the same as in Fig. 1. Dashed lines correspond to the scaling  $K^{-2}$ .

## VI. DISCUSSION

We have proposed a mechanism to suppress heating in aperiodically kicked systems by introducing self-similar multipolar structures. It effectively blocks a series of heating channels and leads to a long-lived prethermal regime even in the absence of TTS and away from the high-frequency regime.

To demonstrate this mechanism, we have considered classical many-body rotor systems and discovered a characteristic prethermal lifetime scaling of  $K^{-2n}$ . In the quasiperiodic TM limit, heating suppression becomes nonperturbative and follows the scaling in Eq. (10), which is neither exponential nor algebraic. A similar functional form has been rigorously proven in the high-frequency regime [60]. It remains an interesting open question to justify such a dependence on the kicking strength.

The Hamiltonian in Eq. (7) can be experimentally realized, e.g., using an array of bosonic Josephson junctions [42,69,70], opening up possibilities for the experimental exploration of prethermalization with RMD kicks. While heating channels can always be suppressed by the RMD sequence, the prethermal lifetime scaling exponent can strongly depend on the microscopic details of the kicked system. The strong dependence of the multipolar order  $n$  may not occur if interaction terms are also present in the static Hamiltonian, such as  $H = H_{\text{kin}} + V_{\text{int}}$ . The leading-order perturbation  $\Omega_{n,1}$  involves terms with more than one  $V_{\text{int}}$ , e.g.,  $\{V_{\text{int}}, \{V_{\text{int}}, H_{\text{kin}}\}\} \sim \sum_j [\sin(q_j - q_{j+1}) - \sin(q_{j-1} - q_j)]^2$ . These terms are independent of angular momenta and cannot be suppressed even at low prethermal temperatures. Hence, the condition in Eq. (3) cannot be satisfied in this case.

Simulating the time evolution with a static interaction requires discretizing the continuous EOMs, which significantly increases the numerical cost for long simulations of the dynamics. Therefore, we modify the kick amplitude of the interaction  $V$  as  $K_l = \pm K + B$ , such that the additional interaction  $V_{\text{int}}$  can be approximately generated at stroboscopic times with a low numerical cost. In Fig. 3(a), we illustrate

the results with  $B = 0.01$ . The prethermal plateau is still observed, and the corresponding lifetime is shown in panel (b). It is evident that, for  $n > 0$ , heating can still be significantly suppressed. However, its dependence on the kicking strength now follows  $t^* \sim (1/K)^2$  regardless of the multipolar order. A similar linearization analysis can be performed, and the expansion rate for each decoupled oscillator is  $K^2$ , as detailed in Appendix G3. Identifying a general mechanism for further suppressing heating with a better scaling remains an intriguing open question.

Finally, we highlight that the perturbative expansion, which predicts the suppression of heating, also applies to RMD kicked quantum systems. A systematic investigation of quantum thermalization in such systems and its connection to their classical counterparts poses an intriguing avenue for future research.

## ACKNOWLEDGMENTS

We thank Marin Bukov, Johannes Knolle, Holger Kantz, Roland Ketzmerick, Paul Schindler, and Yujie Liu for many useful discussions. This paper is supported in part by the Deutsche Forschungsgemeinschaft under cluster of excellence ct.qmat (EXC 2147, Project-ID No. 390858490).

## APPENDIX A: MANY-BODY EFFECTIVE HAMILTONIAN FOR KICKED SYSTEMS

For the quantum kicked system, we have two different unitary time evolution operators:

$$U_0^+ = e^{-i\tau H} e^{-iKV}, \quad U_0^- = e^{-i\tau H} e^{iKV}. \quad (\text{A1})$$

One can obtain a time-averaged Hamiltonian  $H_{\text{ave}}^\pm = H \pm \frac{K}{\tau} V$  as the effective Hamiltonian to approximate the early time dynamics. However, this is not a suitable expansion if  $\tau$  is not sufficiently small and one wants to study the perturbative expansion with respect to the kick strength  $K$ . For instance, the terms  $[H, V]_s$  all have an amplitude scaling of  $O(K)$ , but they are not captured in the averaged Hamiltonian. Instead, it is necessary to perform the replica resummation, whose general expression can be cumbersome to obtain, but there is a systematic approach to achieve it [15], see also examples in Ref. [16]. For the same reason, the previous heating analysis on RMD systems in the high-frequency regime and the expansion of order  $O(\tau)$  will not be applicable here.

To explore the heating effect in RMD kicked systems, we consider the expansion in  $O(K)$  as  $H_n^\pm = \sum_{m=0}^{\infty} K^m \Omega_{n,m}^\pm$  such that  $U_n^\pm = \exp(-i2^n \tau H_n^\pm)$ . The symmetry  $H_n^+ \rightarrow H_n^-$  (under  $K \rightarrow -K$ ) implies that

$$\Omega_{n,m}^+ = (-1)^m \Omega_{n,m}^- := \Omega_{n,m} \quad (\text{A2})$$

for all  $n$ . For  $n = 0$ , a systematic method has been established for constructing the expansion  $U_0^\pm = \exp\{-i\tau[H_0 \pm K\Omega_{0,1} + O(K^2)]\}$ , and the  $O(K)$  term is presented in Eq. (1) [15]. For larger values of  $n$ , we still begin by considering the leading-order correction with  $m = 1$ , and we assume a general

structure for  $n \geq 1$  as

$$\Omega_{n,1}^{\pm} = \sum_{s=0}^{\infty} f_{n,s}^{\pm} \tau^s [H, \Omega_{0,1}]_s, \quad [H, \Omega_{0,1}]_s := \underbrace{[H, \dots, [H, \Omega_{0,1}] \dots]}_s. \quad (\text{A3})$$

From Eq. (A2), we know, for any  $n$  and  $s$ , we have  $f_{n,s}^+ = -f_{n,s}^-$  for  $m = 1$ . Note, we do not require the specific expression for each coefficient  $f_{n,s}^{\pm}$ . Instead, it suffices to demonstrate that some of them become exactly zero, thereby prohibiting certain heating channels. A similar expansion can be derived for higher-order multipolar operators:

$$U_{n+1}^{\mp} = U_n^{\pm} U_n^{\mp} = \exp \left\{ -i2^{n+1} \tau \left[ H + K(f_{n,s}^{\pm} + f_{n,s}^{\mp}) \sum_{s=0}^{\infty} \frac{\tau^s [H, \Omega_{0,1}]_s}{2} \right. \right. \\ \left. \left. - (-i2^{n-1}) K \sum_{s=0}^{\infty} \tau^{s+1} f_{n,s}^{\pm} [H, \Omega_{0,1}]_{s+1} + K \sum_{l=2}^{\infty} \sum_{s=0}^{\infty} \tau^{s+l} g_{n,s,l}^{\pm} [H, \Omega_{0,1}]_{s+l} + O(K^2) \right] \right\}, \quad (\text{A4})$$

where  $g_{n,s,l}$  are some coefficients, and importantly,  $f_{n,s}^{\pm} + f_{n,s}^{\mp} = 0$  in the first line cancels. By comparing it with the assumption in Eq. (A3) but for  $n = 1$ , we have

$$U_{n+1}^{\mp} = \exp \left\{ -i2^{n+1} \tau \left[ H + K \sum_{s=0}^{\infty} \tau^s f_{n+1,s}^{\mp} [H, \Omega_{0,1}]_s \right] + O(K^2) \right\}, \quad (\text{A5})$$

and by matching the coefficients of  $\tau^s$ , we can establish the following relation for the coefficients:

$$\begin{aligned} f_{n,s}^+ &= 0, & \text{for } s \leq n-1, \\ f_{n,s}^+ &= (-i)2^{n-2} f_{n-1,s-1}^+, & \text{for } s = n, \end{aligned} \quad (\text{A6})$$

and obtaining  $f_{n,s}^+$  for  $s \geq n+1$  can be cumbersome. Therefore, the first line in Eq. (A6) implies Eq. (6) in the main text. It suggests that, to the leading order of  $O(K)$ , heating can only occur via the process  $[H, V]_s$  with  $s \geq n$ , while all other heating channels are strictly forbidden.

Higher-order terms with an even order of  $K$  do not introduce random perturbations. However, they still contribute to heating in the form of Arnold diffusion, like periodically driven systems, but their contribution is exponentially small in the kick strength [43]. As a result, the next significant random heating channels emerge at order  $O(K^3)$ . It can also be shown that the self-similarity of the RMD sequence leads to the exact suppression of these heating channels. To see this more easily, we consider a special case where higher-order nested commutators have negligible contributions:

$$[H, V]_s = 0, \quad (\text{A7})$$

for  $\forall s \geq n_c$  with a certain integer  $n_c$ . Consequently,  $\Omega_{n,1} = 0$ , and the stroboscopic time evolution of the system is effectively governed by the Hamiltonian  $H_n^{\pm} = H + K^2 \Omega_{n,2} \pm K^3 \Omega_{n,3} + O(K^4)$ , where

$$\Omega_{n,3} = \sum_{s=0}^{\infty} h_{n,s} \tau^s [H, \Omega_{k,3}]_s, \quad (\text{A8})$$

for  $n > k$  and a certain integer  $k$ . By using  $U_{n+1}^{\mp} = U_n^{\pm} U_n^{\mp}$ , one can again observe the vanishing coefficients:

$$h_{n,s} = 0, \quad \text{for } s \leq n-k-1, \quad n \geq k+1. \quad (\text{A9})$$

## APPENDIX B: SIMULATIONS FOR HIGH-FREQUENCY DRIVE

Figure 4 depicts dynamics for a fixed kick strength  $K$  and varying kick period  $\tau$  with  $n = 1$  random multipolar sequence. Kinetic energy increases faster when  $\tau$  becomes smaller, indicating that the high-frequency limit cannot suppress heating for this particular set of driving parameters. Note, the interplay between the  $\tau \rightarrow 0$  and  $K \rightarrow 0$  limits is unclear and worthy of systematic study in the future.

## APPENDIX C: TEMPERATURE AT THE PRETHERMAL STAGE

Here, we analyze the dependence of the prethermal temperature on the kick strength, and we demonstrate that it follows  $T \sim K^2$ . For the initial condition  $p_j = \bar{p}$ , the initial kinetic energy density is given by  $\bar{p}^2/2$ . In the prethermal regime with a weak kick, we assume that the distribution for  $p_j$  and  $q_j$  decouples [43]. The angular momentum distribution approaches

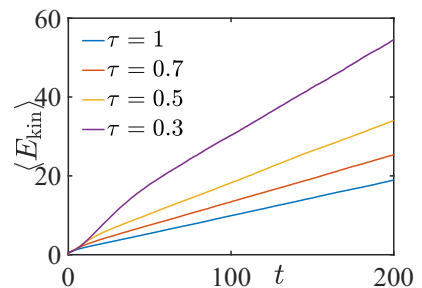


FIG. 4. Time evolution of the averaged kinetic energy for different kick periods  $\tau$ . Reducing  $\tau$  clearly increases the heating rate. We use  $n = 1$  random multipolar drive (RMD) and a fixed kick strength  $K = 0.5$ .  $q_j(0)$  is generated from a random uniform sampling within  $[0, 2\pi]$ , and  $p_j(0)$  is randomly chosen from a Gaussian distribution with zero mean and standard deviation  $\sigma = 1$ . Different values of the kick period  $\tau$  are shown in the legend.

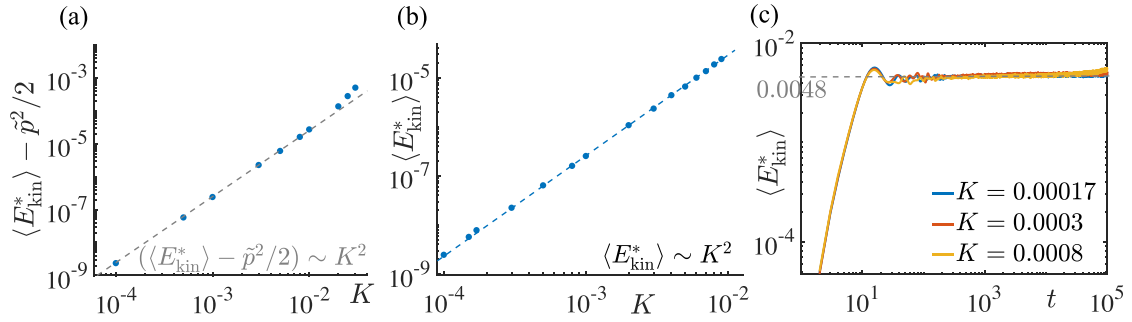


FIG. 5. The averaged prethermal kinetic energy density  $\langle E_{\text{kin}}^* \rangle$  for  $n = 1$  random multipolar drive (RMD) for (a)  $B = 0$  with  $\tilde{p} = 0.1$ , (b)  $B = 0$  with  $\tilde{p} = 0$ , and (c)  $B = 0.01$  with  $\tilde{p} = 0$ . The prethermal temperature scales as  $T \sim K^2$  for (a) and (b) when the kick is weak. In the last case, it is fixed by  $B$ , so all the plateau parts of energy curves are at the same value  $\langle E_{\text{kin}}^* \rangle = 0.0048$ . The rest numerical settings are the same as in Fig. 1. All plots use a log-log scale.

the Gibbs distribution  $Z^{-1} \prod_{j=1}^N \exp[-(p_j - \tilde{p})^2/2T]$  with a normalization factor  $Z^{-1}$ . The corresponding kinetic energy density is  $E_{\text{kin}}^* = (T + \tilde{p}^2)/2$ . We numerically study the dependence of the temperature  $T$  on the kick strength  $K$  in Figs. 5(a) and 5(b) for two different initial conditions:  $\tilde{p} = 0.1$  and  $\tilde{p} = 0$ , respectively. The numerical results fit well with a straight line in a log-log scale, with a slope  $\sim 2$ . This suggests that the temperature follows  $T \sim K^2$ .

In contrast, for the modified kicked protocol used in Fig. 3 with a nonvanishing  $B$ , the averaged prethermal kinetic energy linearly depends on  $B$  but does not notably change with  $K$ . We verify this in Fig. 5(c).

#### APPENDIX D: DETAILS ON NUMERICAL SIMULATION SETTINGS

Figure 1: The discrete classical EOMs in Eq. (9) are used to simulate individual trajectories. For each fixed  $n$  and fixed  $K$ , each set of initial conditions is given by  $q_j(0) \sim \text{Uni}[0, 2\pi]$  with  $p_j(0) = 0.1$ ,  $j = 1, 2, \dots, 500$ ; for each initial point, we assign a random noise realization according to the random multipolar driving protocol, and the kinetic energy  $\langle E_{\text{kin}} \rangle$  is averaged over 350 noise realizations and  $N = 500$  rotors. We perform the same simulation for  $n = 0, 1, 2, 3$ , and 20 [TM in Fig. 1(a)] and plot  $\langle E_{\text{kin}} \rangle$  as a function of time. The lifetime  $t^*$  is then extracted in the following way: Fit the  $\langle E_{\text{kin}} \rangle$  curve up to time  $t_f$  with a power law  $t^b$  and monitor the power  $b$  for different  $t_f$ ;  $t^* = t_f$  when  $b$  reaches the threshold 0.05. We extract  $t^*$  for each  $n$  and each  $K$  and plot in dots with different colors in Figs. 1(b) and 1(c).

Figure 2: The linearized EOM in Eq. (12) is used with the matrix  $M_1^\pm$  corresponding to the multipolar order  $n = 1$ . We choose  $F = 0.08$ ; in Fig. 2(a), the black ellipse [ $r_0 = 0.1$ , cf. Eq. (G15)] is determined by the averaged normalized matrix  $\bar{M}_1^\pm$ . The magenta curve is generated by a trajectory starting from an arbitrary point on the black ellipse and iterated according to the averaged matrix  $\bar{M}_1^\pm$  for time  $h \leq 300$ , and the blue curve is generated by a trajectory starting at the same point but iterated according to a random sequence of  $M_1^\pm$  (with equal probability). In Fig. 2(b), the blue dots are the averaged radius  $\langle r_h \rangle$  computed along the blue trajectory in Fig. 2(a) at different times  $h$ , similarly for the orange dots except  $n = 2$ ; the dashed lines are predictions from our linearization theory, cf. Eqs. (G19)–(G21).

#### APPENDIX E: PERIODICALLY KICKED ROTOR SYSTEMS

The periodically driven many-body rotor system has been studied in previous literature, e.g., Ref. [43], and we reproduced their main results in Fig. 6. The evolution of averaged kinetic energy exhibits a scaling of the prethermal lifetime which is exponential for Floquet systems, as shown in Fig. 6(b), rather than the algebraic scaling as presented in this paper.

#### APPENDIX F: SCALING OF THE THUE-MORSE PRETHERMAL LIFETIME

In the main text, we show that, for the TM drive, the lifetime scaling becomes  $t^* \sim \exp\{C[\ln(K^{-1}/g)]^2\}$  with constants  $C$  and  $g$ . Here, we compare this result with other fitting methods. For instance, in Fig. 7(a), we use a log-log scale, and clearly, the numerical data tend to curve up. In contrast, panel (b) depicts the same data but in log scale, and the numerical result bends down. Therefore, this scaling grows faster than any power law but slower than exponentially.

#### APPENDIX G: LINEARIZATION OF THE MANY-BODY HAMILTONIAN

##### 1. Time evolution matrix

Following Ref. [71], we can express the Hamiltonian of our model as a collection of decoupled kicked harmonic

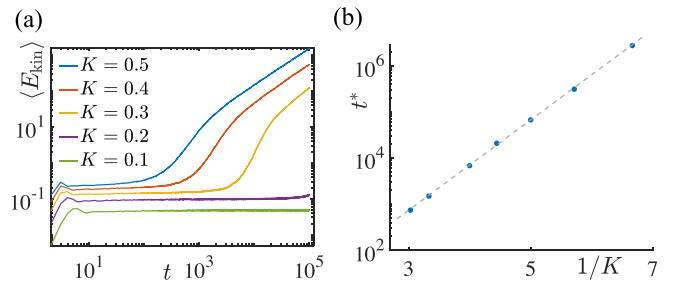


FIG. 6. Prethermalization for the periodically driven case: (a) averaged kinetic energy vs time in a log-log scale, and (b) prethermal lifetime  $t^*$  vs  $1/K$  in a semilog scale.

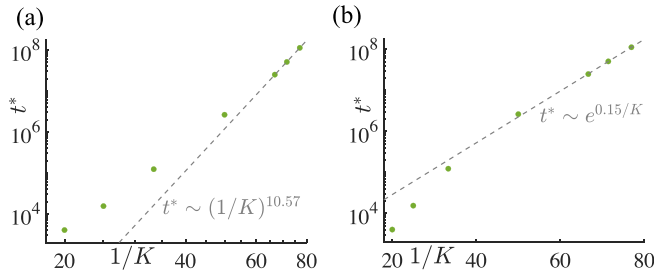


FIG. 7. (a) and (b) depict the power-law and exponential fitting of the prethermal lifetime  $t^*(1/K)$  for the Thue-Morse (TM) drive.

oscillators in a quadratic approximation:  $\cos(q_j - q_{j+1}) \approx 1 - (q_j - q_{j+1})^2/2$ , provided that the two neighboring rotor angles are sufficiently close  $(q_j - q_{j+1}) \bmod 2\pi \approx 0$ . Thus,

we have

$$H(t) = \sum_{j=1}^N \left[ \frac{p_j^2}{2} - (B \pm K) \cos(q_j - q_{j+1}) \sum_{l=-\infty}^{+\infty} \delta(t - l\tau) \right] \\ \approx \frac{1}{2} \sum_w \left[ |P_w|^2 + F^\pm(w) |Q_w|^2 \sum_{l=-\infty}^{+\infty} \delta(t - l\tau) \right], \quad (\text{G1})$$

where  $w := 2\pi I/N$ ,  $F^\pm(w) := 4(B \pm K) \sin^2(w/2)$  [the choice of  $F^\pm(w)$  depends on the RMD sequence], and  $P_w = \frac{1}{\sqrt{N}} \sum_{j=1}^N p_j e^{-iwj}$  and  $Q_w = \frac{1}{\sqrt{N}} \sum_{j=1}^N q_j e^{-iwj}$  are the Fourier transforms of  $p_j$  and  $q_j$ , respectively. Note that Eq. (11) in the main text is a simplified version of the Hamiltonian above with  $B = 0$ . Here, we use the general expression with nonzero  $B$  such that the linear stability of the dynamics in Fig. 3 can also be discussed.

Since  $p_j$  and  $q_j$  are real, we have  $P_w^* = P_{-w}$  and  $Q_w^* = Q_{-w}$  (here, a star denotes a complex conjugate). For each  $w$ , the classical EOMs are given by

$$\frac{d}{dt} \begin{pmatrix} Q_w \\ Q_{-w} \\ P_w \\ P_{-w} \end{pmatrix} = \begin{pmatrix} P_{-w} \\ P_w \\ -F^\pm(w)\Omega(t)Q_{-w} \\ -F^\pm(w)\Omega(t)Q_w \end{pmatrix} = \begin{pmatrix} 0 & 0 & 0 & 1 \\ 0 & 0 & 1 & 0 \\ 0 & -F^\pm(w)\Omega(t) & 0 & 0 \\ -F^\pm(w)\Omega(t) & 0 & 0 & 0 \end{pmatrix} \begin{pmatrix} Q_w \\ Q_{-w} \\ P_w \\ P_{-w} \end{pmatrix} =: M^\pm(t) \begin{pmatrix} Q_w \\ Q_{-w} \\ P_w \\ P_{-w} \end{pmatrix}, \quad (\text{G2})$$

where  $\Omega(t) = \sum_{k=-\infty}^{+\infty} \delta(t - k\tau)$ .

Consider the evolution of the system over one time period, from  $t = -\epsilon$  to  $t = \tau - \epsilon$  with  $\epsilon \ll \tau$ . The solution to the above equation is

$$\begin{pmatrix} Q_w(\tau - \epsilon) \\ Q_{-w}(\tau - \epsilon) \\ P_w(\tau - \epsilon) \\ P_{-w}(\tau - \epsilon) \end{pmatrix} \sim \exp \left[ \int_{-\epsilon}^{\tau - \epsilon} M^\pm(t) dt \right] \begin{pmatrix} Q_w(-\epsilon) \\ Q_{-w}(-\epsilon) \\ P_w(-\epsilon) \\ P_{-w}(-\epsilon) \end{pmatrix}. \quad (\text{G3})$$

During the first part of the period [when  $t \in (-\epsilon, \epsilon)$ ], the rotor is kicked, and the time evolution is determined by the matrix:

$$M_{\text{kick},w}^\pm = \lim_{\epsilon \rightarrow 0} \exp \left[ \int_{-\epsilon}^{+\epsilon} M^\pm(t) dt \right] = \exp \begin{pmatrix} 0 & 0 & 0 & 0 \\ 0 & 0 & 0 & 0 \\ 0 & -F^\pm(w) & 0 & 0 \\ -F^\pm(w) & 0 & 0 & 0 \end{pmatrix} = \begin{pmatrix} 1 & 0 & 0 & 0 \\ 0 & 1 & 0 & 0 \\ 0 & -F^\pm(w) & 1 & 0 \\ -F^\pm(w) & 0 & 0 & 1 \end{pmatrix}. \quad (\text{G4})$$

In the second part of the time period [when  $t \in (\epsilon, \tau - \epsilon)$ ], the rotor experiences a free motion, described by the matrix (with  $\epsilon \rightarrow 0$ ):

$$M_{\text{free}} = \begin{pmatrix} 1 & 0 & 0 & \tau \\ 0 & 1 & \tau & 0 \\ 0 & 0 & 1 & 0 \\ 0 & 0 & 0 & 1 \end{pmatrix}. \quad (\text{G5})$$

As a result, the phase space evolution of the kicked rotor over one time period is given by the matrix:

$$M_w^\pm = M_{\text{free}} M_{\text{kick},w}^\pm = \begin{pmatrix} 1 - F^\pm(w)\tau & 0 & 0 & \tau \\ 0 & 1 - F^\pm(w)\tau & \tau & 0 \\ 0 & -F^\pm(w) & 1 & 0 \\ -F^\pm(w) & 0 & 0 & 1 \end{pmatrix}. \quad (\text{G6})$$

Notice that the matrix  $M_w^\pm$  can be reduced to a  $2 \times 2$  matrix:

$$M_0^\pm = \begin{pmatrix} 1 - \tau F^\pm & \tau \\ -F^\pm & 1 \end{pmatrix}, \quad (\text{G7})$$



where the subscript  $w$  is dropped from now on. The evolution matrices for higher multipolar orders  $n$  can be derived recursively as  $M_n^\pm = M_{n-1}^\mp M_{n-1}^\pm$ , which determines the time evolution of duration  $2^n \tau$ . For example, when  $B = 0$ ,  $n = 1$ , we have

$$\begin{aligned} M_1^+ &= \begin{pmatrix} -\tau^2 F^2 - \tau F + 1 & \tau^2 F + 2\tau \\ -\tau F^2 & \tau F + 1 \end{pmatrix}, \\ M_1^- &= \begin{pmatrix} -\tau^2 F^2 + \tau F + 1 & -\tau^2 F + 2\tau \\ -\tau F^2 & -\tau F + 1 \end{pmatrix}, \end{aligned} \quad (\text{G8})$$

where we have denoted  $F := F^+ = -F^-$ .

## 2. Stability of integrable orbits

We use the method proposed in Ref. [67] to analyze the stability of the elliptical orbits. Let us denote

$$\bar{M}_n := \frac{1}{2}(M_n^+ + M_n^-) \quad \text{and} \quad D_n := \frac{1}{2}(M_n^+ - M_n^-), \quad (\text{G9})$$

such that  $M_n^\pm = \bar{M}_n + \xi D_n$ , where  $\xi$  is a random variable, being either  $+1$  or  $-1$  with the same probability. Hence, its average vanishes  $\langle \xi \rangle = 0$ , and the variance reads  $\langle \xi^2 \rangle = 1$ . We note that  $\det(\bar{M}_n) = 1 + O((\tau F)^{2n})$  for nonzero  $n$ , implying that the averaged map  $\bar{M}_n$  is not area-preserving. We therefore define a new matrix  $\bar{M}' := \bar{M}_n / \sqrt{\det \bar{M}_n}$  so that  $\det(\bar{M}') = 1$ , and this new matrix can be used to define the area of a closed orbit in the linearized system. This orbit is generally a rotated ellipse centered around the fixed point  $(0, 0)$ . Note,  $\bar{M}'$  also depends on the multipolar order  $n$ , but the following method equally applies for all  $n$ . For now, we drop it for simplicity. With the matrix elements  $M_{ij}$  of  $\bar{M}'$ , its area can be defined as [72]

$$A(Q_w, P_{-w}) = \frac{\pi [M_{12} P_{-w}^2 - M_{21} Q_w^2 + (M_{11} - M_{22}) Q_w P_{-w}]}{\sqrt{1 - \left(\frac{M_{11} + M_{22}}{2}\right)^2}}, \quad (\text{G10})$$

which is conserved if  $\bar{M}'$  is repeatedly applied. Here,  $Q_w$  and  $P_{-w}$  are generally time dependent, and in the following, we drop  $w$  for simplicity and introduce  $h$  to label their time dependence. We only focus on stroboscopic time evolution and use  $(Q_h, P_h)$  to represent the trajectory at time  $h2^n \tau$ . One can use the polar angle  $\phi_h$  to parameterize the points  $(Q_h, P_h)$  on the rotated ellipse as

$$Q_h = R_q \cos(\theta) \cos(\phi_h) - R_p \sin(\theta) \sin(\phi_h), \quad (\text{G11})$$

$$P_h = R_q \sin(\theta) \cos(\phi_h) + R_p \cos(\theta) \sin(\phi_h), \quad (\text{G12})$$

where  $R_{q/p}$  defines the length of the major or minor axis, and  $\theta$  defines the rotation angle with respect to the axis. It can be determined by

$$\tan(2\theta) = -\frac{M_{11} - M_{22}}{M_{12} + M_{21}}. \quad (\text{G13})$$

One can also convert the variables back as

$$\cos \phi_h = \frac{Q_h \cos \theta + P_h \sin \theta}{R_q}, \quad \sin \phi_h = \frac{-Q_h \sin \theta + P_h \cos \theta}{R_q}. \quad (\text{G14})$$

The lengths of the major and minor axes are given by

$$\begin{aligned} R_q &= \frac{\sqrt{2} r_0}{\beta} \left[ \frac{M_{11} - M_{22}}{\sin 2\theta} + M_{12} - M_{21} \right]^{-1/2}, \\ R_p &= \frac{\sqrt{2} r_0}{\beta} \left[ -\frac{M_{11} - M_{22}}{\sin 2\theta} + M_{12} - M_{21} \right]^{-1/2}, \end{aligned} \quad (\text{G15})$$

with the constant:

$$\beta := \left[ 1 - \frac{(M_{11} + M_{22})^2}{4} \right]^{-1/4}. \quad (\text{G16})$$

It is worth noting that, for  $n = 1$ ,  $R_q \sim O(F^{-1})$ ,  $R_p \sim O(F^0)$ , so for a weak kick strength,  $R_q$  can be large. This stretches the ellipse in the  $Q$  direction much more strongly than in the  $P$  direction.

For RMD drives where  $M_n^\pm$  is applied stochastically, the area of the closed orbit becomes time dependent. For a single random realization and at a certain time, this area can either expand or contract. However, if we average over many different random realizations, it generally expands. We can quantify this expansion by first defining the radius of the ellipse  $r_h = \sqrt{A(Q_h, P_h)}/\pi$  and calculating the expansion rate  $\Delta r_h / r_h$ , where  $\Delta r_h := r_{h+1} - r_h$ . We use the same metric to define the area of the ellipse, but now the trajectory updates stochastically as

$$\begin{pmatrix} Q_{h+1} \\ P_{h+1} \end{pmatrix} = M_n^\pm(w) \begin{pmatrix} Q_h \\ P_h \end{pmatrix}. \quad (\text{G17})$$

The expansion rate now reads

$$\frac{\Delta r_h}{r_h} := \frac{r_{h+1}}{r_h} - 1 = \sqrt{\frac{M_{12} P_{h+1}^2 - M_{21} Q_{h+1}^2 + (M_{11} - M_{22}) Q_{h+1} P_{h+1}}{M_{12} P_h^2 - M_{21} Q_h^2 + (M_{11} - M_{22}) Q_h P_h}} - 1. \quad (\text{G18})$$

We now insert Eq. (G17) into Eq. (G18) to obtain the general expression as a function of the polar angle  $\phi_h$ , the kick strength  $F$ , and the kick duration  $\tau$ . Unfortunately, it is usually very complicated and not enlightening. However, if the kick strength  $F$  is small, one can perform a Taylor expansion to obtain the most relevant contributions. For our purpose, a Taylor expansion up to the order  $O(F^{2n})$  would be sufficient. This process can be done by employing symbolic computation tools such as Wolfram Mathematica.

For  $n = 1$ , to the second order of  $F$ , we have

$$\frac{\Delta r_h}{r_h} \approx \left( \tau F \cos 2\phi_h + \tau^2 F^2 \frac{\sqrt{2}}{2} \sin 2\phi_h \right) \xi + [1 + \xi^2 (1 - \cos^2 2\phi_h)] \frac{\tau^2 F^2}{2}. \quad (\text{G19})$$

Terms that are linear in  $\xi$  vanish after averaging over different random realizations. Contributions that are quadratic in  $\xi$  generally do not vanish, unless for special polar angles, e.g.,  $\cos^2 2\phi_h = 1$ . Also note that there is a term of order  $O(F)$  which does not depend on  $\xi$ . It arises from the fact that the average map  $\bar{M}_n$  is not area-preserving, contributing a constant expansion rate, as shown in Fig. 2 (the magenta line).

To further remove the angular dependence in the expansion rate, one can assume that the change in the radial direction is much slower than in the angular direction and integrate the angle  $\phi_h$  over the full range  $[0, 2\pi]$ . We further use  $\langle \xi \rangle = 0$

and  $\langle \xi^2 \rangle = 1$  to obtain the averaged expansion rate that is proportional to  $F^2$ :

$$\left\langle \frac{\Delta r_h}{r_h} \right\rangle = \frac{1}{2\pi} \int_0^{2\pi} \frac{\Delta r_h}{r_h} d\phi_h \approx \frac{1}{4} \tau^2 F^2 (2 + \langle \xi^2 \rangle) = \frac{3}{4} \tau^2 F^2. \quad (\text{G20})$$

This provides an approximation for the mean radius evolution for small  $h$  (and small  $\tau F$ ):  $\langle r_h \rangle \approx r_0 (1 + \frac{3}{4} \tau^2 F^2 h)$ .

Similarly for  $n = 2$ :

$$\frac{\Delta r_h}{r_h} \approx \left[ \left( \frac{37\sqrt{2}}{8} \tau^2 F^2 - 2\sqrt{2} \right) \tau^2 F^2 \sin 2\phi_h - 6\tau^3 F^3 \cos 2\phi_h \right] \xi + (2\xi^2 \cos 4\phi_h + 2\xi^2 + 4) \tau^4 F^4, \quad (\text{G21})$$

and  $\langle \frac{\Delta r_h}{r_h} \rangle \approx 2(2 + \langle \xi^2 \rangle) \tau^4 F^4 = 6\tau^4 F^4$ .

Lastly for  $n = 3$ , to the sixth order of  $F$ :

$$\begin{aligned} \frac{\Delta r_h}{r_h} \approx & \left( -16\tau^3 F^3 \cos 2\phi_h + 56\sqrt{2}\tau^4 F^4 \sin 2\phi_h + 206\tau^5 F^5 \cos 2\phi_h - \frac{429\sqrt{2}}{2} \tau^6 F^6 \sin 2\phi_h - 2\sqrt{2}\tau^4 F^6 \sin 4\phi_h \right) \xi \\ & + (-\xi^2 \cos 4\phi_h + \xi^2 + 2) 64\tau^6 F^6, \end{aligned} \quad (\text{G22})$$

and the average  $\langle \frac{\Delta r_h}{r_h} \rangle \approx 64(2 + \langle \xi^2 \rangle) \tau^6 F^6 = 192\tau^6 F^6$ .

### 3. Eigenvalues of the matrices $\bar{M}_n$ and $D_n$

Instead of rigorously calculating the expansion rates and their dependence on  $n$ , one can also estimate them by studying the scaling of eigenvalue properties of the update matrix. We first assume  $B = 0$  and then obtain  $\bar{M}_n$  recursively as

$$\bar{M}_0 = \begin{pmatrix} 1 & \tau \\ 0 & 1 \end{pmatrix}, \quad (\text{G23})$$

$$\bar{M}_1 = \begin{pmatrix} 1 - \tau^2 F^2 & 2\tau \\ -\tau F^2 & 1 \end{pmatrix}, \quad (\text{G24})$$

$$\bar{M}_2 = \begin{pmatrix} 1 - 5\tau^2 F^2 + \tau^4 F^4 & 2\tau(2 - \tau^2 F^2) \\ \tau F^2(-2 + \tau^2 F^2) & 1 - 3\tau^2 F^2 \end{pmatrix}, \quad (\text{G25})$$

$$\bar{M}_3 = \begin{pmatrix} 1 - 18\tau^2 F^2 + 27\tau^4 F^4 - 11\tau^6 F^6 + \tau^8 F^8 & 2\tau(4 - 18\tau^2 F^2 + 10\tau^4 F^4 - \tau^6 F^6) \\ \tau F^2(-4 + 18\tau^2 F^2 - 10\tau^4 F^4 + \tau^6 F^6) & 1 - 14\tau^2 F^2 + 9\tau^4 F^4 - \tau^6 F^6 \end{pmatrix}, \quad (\text{G26})$$

with eigenvalues

$$\bar{\lambda}_{0,\pm} = 1, \quad (\text{G27})$$

$$\bar{\lambda}_{1,\pm} = \left( 1 - \frac{1}{2} \tau^2 F^2 \right) \pm \left( -\frac{1}{2} \tau F \right) \sqrt{-8 + \tau^2 F^2}, \quad (\text{G28})$$

$$\bar{\lambda}_{2,\pm} = \left( 1 - 4\tau^2 F^2 + \frac{1}{2} \tau^4 F^4 \right) \pm \left( -\tau F + \frac{1}{2} \tau^3 F^3 \right) \sqrt{-8 + \tau^2 F^2}, \quad (\text{G29})$$

$$\bar{\lambda}_{3,\pm} = \left( 1 - 16\tau^2 F^2 + 18\tau^4 F^4 - 6\tau^6 F^6 + \frac{1}{2} \tau^8 F^8 \right) \pm \left( -2\tau F + 9\tau^3 F^3 - 5\tau^5 F^5 + \frac{1}{2} \tau^7 F^7 \right) \sqrt{-8 + \tau^2 F^2}. \quad (\text{G30})$$

Since  $\tau^2 F^2 \ll 8$ , the eigenvalues of  $\bar{M}_n$  for each  $n > 0$  form a complex conjugate pair. Furthermore, as  $\det(\bar{M}_n) > 1$ , the deviation from one determines the rate of constant expansion of the dynamics generated by  $\bar{M}_n$ . Specifically, we calculate  $\sqrt{\det(\bar{M}_n)}$  for different values of  $n$ , which correspond to the norms of the eigenvalues of  $M_n$ :

$$|\bar{\lambda}_{1,\pm}| = 1 + \frac{1}{2} (\tau F)^2 - \frac{1}{8} (\tau F)^4 + O((\tau F)^6), \quad (\text{G31})$$

$$|\bar{\lambda}_{2,\pm}| = 1 + 4(\tau F)^4 - \frac{1}{2} (\tau F)^6 + O((\tau F)^8), \quad (\text{G32})$$

$$|\bar{\lambda}_{3,\pm}| = 1 + 128(\tau F)^6 - 160(\tau F)^8 + O((\tau F)^{10}). \quad (\text{G33})$$

Note that, for a weak kick strength, we have  $(|\bar{\lambda}_{n,\pm}| - 1) \sim (\tau F)^{2n}$  for a small value of  $n$ , and higher-order terms are negligible. Therefore, we expect the constant expansion rate to scale as  $F^{2n}$ , as discussed in the previous section Appendix G 2. However, we also observe that the prefactor for higher powers of  $F$  tends to increase for  $n = 3$ , suggesting that the perturbative expansion in orders of  $F$  may not converge for a large value of  $n$ .

We also compute the matrix  $D_n$ :

$$D_0 = \begin{pmatrix} -\tau F & 0 \\ -F & 0 \end{pmatrix}, \quad (\text{G34})$$

$$D_1 = \begin{pmatrix} \tau F & -\tau^2 F \\ 0 & -\tau F \end{pmatrix}, \quad (\text{G35})$$

$$D_2 = \begin{pmatrix} \tau^3 F^3 & \tau^2 F(4 - \tau^2 F^2) \\ 2\tau^2 F^3 & -\tau^3 F^3 \end{pmatrix}, \quad (\text{G36})$$

$$D_3 = \begin{pmatrix} -16\tau^3 F^3 + 10\tau^5 F^5 - \tau^7 F^7 & \tau^4 F^3(16 - 10\tau^2 F^2 + \tau^4 F^4) \\ 0 & 16\tau^3 F^3 - 10\tau^5 F^5 + \tau^7 F^7 \end{pmatrix}; \quad (\text{G37})$$

with eigenvalues

$$\mu_{0,\pm} = 0, -\tau F, \quad (\text{G38})$$

$$\mu_{1,\pm} = \mp \tau F, \quad (\text{G39})$$

$$\mu_{2,\pm} = \pm \tau^2 F^2 \sqrt{8 - \tau^2 F^2}, \quad (\text{G40})$$

$$\mu_{3,\pm} = \pm (16\tau^3 F^3 - 10\tau^5 F^5 + \tau^7 F^7), \quad (\text{G41})$$

which scales as  $|\mu_{n,\pm}| \sim (\tau F)^n$  for  $n > 0$ . As  $D_n$  appears stochastically in time, we expect its leading-order contribution to vanish. Its second-order effects lead to a diffusive spiral-out process with an expansion rate that scales as  $F^{2n}$ .

We perform a similar calculation for nonzero  $B$ , and by defining  $F^\pm \sim (\pm K + B)$ , we obtain

$$|\bar{\lambda}_{1,\pm}| = \sqrt{1 + \frac{\tau^4}{4}(F^+ - F^-)^2} = 1 + \frac{\tau^2}{8}(F^+ - F^-)^2 + O((F^+ - F^-)^3), \quad (\text{G42})$$

$$|\bar{\lambda}_{2,\pm}| = 1 + \frac{\tau^3}{8}(F^+ - F^-)^2 [8 - 3\tau(F^+ + F^-) + \tau^2 F^+ F^-] (F^+ + F^- - \tau F^+ F^-) + O((F^+ - F^-)^3), \quad (\text{G43})$$

$$|\bar{\lambda}_{3,\pm}| = 1 + \frac{\tau^4}{8}(F^+ - F^-)^2 (F^+ + F^- - \tau F^+ F^-)^2 [8 - 3\tau(F^+ + F^-) + \tau^2 F^+ F^-]^2 [2 - 2\tau(F^+ + F^-) + \tau^2 F^+ F^-]^2 + O((F^+ - F^-)^3). \quad (\text{G44})$$

Importantly, one always finds  $(|\bar{\lambda}_{n,\pm}| - 1) \sim K^2$ , where the scaling exponent does not depend on the multipolar order. This scaling relation corresponds to the observed heating rate scaling of  $K^2$  in Fig. 3 in the next section.

## APPENDIX H: DISTRIBUTION OF ANGULAR MOMENTA

In the main text, we linearize the many-body Hamiltonian and explain the characteristic scaling of the prethermal lifetime. We note that such scaling can be very stable and persist even away from the linearization regime  $(q_j - q_{j+1}) \bmod 2\pi \ll 1$ , as shown in Fig. 1, where a wide initial distribution of  $q_j$  is used. Interestingly, we notice that this lifetime scaling is not sensitive to the angular dependence but strongly relies on the angular momentum distribution during the prethermal regime. As discussed in Appendix C, this distribution is governed by the prethermal temperature. We find that, as long as the prethermal regime exhibits a low temperature or, equivalently, a narrow distribution of angular

momenta, the prethermal regime can be sufficiently long-lived, and the dependence on  $n$  should manifest.

The prethermal temperature can be adjusted by the initial condition. For instance, we consider an initial angular momentum distribution following a Gaussian distribution with a zero mean and a standard deviation  $\sigma$ . A larger standard deviation generally increases the prethermal temperature, resulting in a broader angular momentum distribution during the prethermal regime. This is confirmed in Fig. 8(a), where three different values of the initial standard deviation  $\sigma$  are used. Note that we use  $n = 1$  to generate the dynamics, but this figure qualitatively represents other multipolar orders as well. The kick strength  $K$  is chosen such that the prethermal lifetimes are approximately the same for all  $\sigma$ , with values of  $K$  set as 0.012, 0.008, and 0.005 for  $\sigma = 0.001, 0.01, \text{ and } 0.1$ , respectively. The probability distributions are extracted at  $t = 1500$  just before the system notably heats up.

We now illustrate the dependence of the prethermal lifetime scaling on different initial conditions, focusing on the

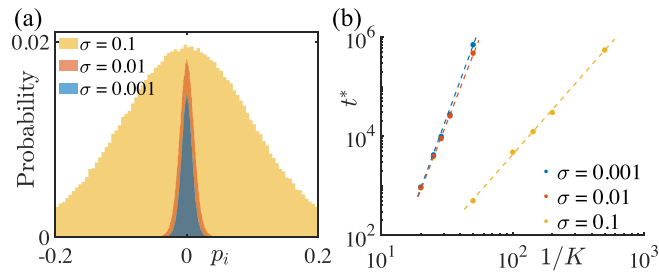


FIG. 8. (a) Momentum distribution at the end of the prethermal stage for a Gaussian initial momentum distribution with a zero mean and a standard deviation  $\sigma$  indicated in different colours, and (b) corresponding prethermal lifetime  $t^*$  as a function of  $1/K$  for  $n = 20$  in log-log. The rest numerical settings are the same as in Fig. 1.

TM drive. For a fixed kick strength  $K$ , it typically determines the longest possible prethermal lifetime for the entire family of  $n$ -RMD protocols. Therefore, if we fit  $t^*$  vs  $1/K$  on a log-log scale, the scaling exponent also sets the upper bound for other  $n$ -RMD protocols. As long as the TM drive exhibits a sufficiently large scaling exponent  $\alpha$ ,  $n$ -RMD with any finite  $n$  should exhibit the  $n$ -dependence in the lifetime scaling.

In Fig. 8(b), we present the prethermal lifetime scaling for different initial conditions. For narrow distributions, such as  $\sigma = 0.001$  and  $0.01$ , the scaling exponents are still very large, approximately  $\alpha \approx 7.9$  and  $7.2$ , respectively. We expect that these fitted scaling exponents may increase further if we perform the fit using larger  $1/K$  and longer time windows, like in Fig. 1(c). However, for a larger standard deviation, such as  $\sigma = 0.1$ , the scaling exponent notably decreases to  $\alpha \approx 3.1$ ,

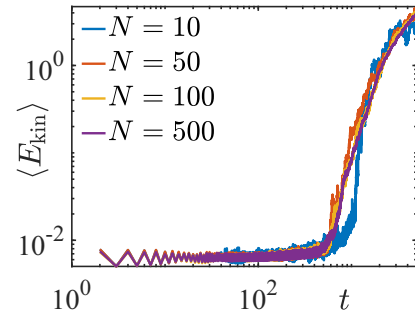


FIG. 9. Time evolution of the averaged kinetic energy for the TM drive. The simulation results converge for large systems, and  $N = 500$  is already sufficient to produce thermodynamically large systems. Here, we use the kick strength  $K = 0.07$ , and the results are averaged over 200 random realizations. Initial states are the same as in Fig. 1.

and we expect that  $n$ -RMD systems with finite  $n$  would heat up faster.

Therefore, we expect that, as long as the prethermal regime has a low temperature, a long-lived prethermal regime and the  $n$ -dependence in the lifetime scaling should emerge. Further systematic investigations of the temperature dependence of the prethermal lifetime scaling will be explored in future work.

#### APPENDIX I: FINITE-SIZE EFFECTS

In Fig. 9, we compare the dynamics using the TM drive for different system sizes. The simulations converge as the system size increases. In the main text, we use  $N = 500$  to generate the data, which is already sufficient to mimic the heating behavior in thermodynamically large systems.

- [1] V. Khemani, R. Moessner, and S. Sondhi, A brief history of time crystals, [arXiv:1910.10745](https://arxiv.org/abs/1910.10745) (2019).
- [2] M. P. Zaletel, M. Lukin, C. Monroe, C. Nayak, F. Wilczek, and N. Y. Yao, Colloquium: Quantum and classical discrete time crystals, *Rev. Mod. Phys.* **95**, 031001 (2023).
- [3] L. D'Alessio and M. Rigol, Long-time behavior of isolated periodically driven interacting lattice systems, *Phys. Rev. X* **4**, 041048 (2014).
- [4] A. Lazarides, A. Das, and R. Moessner, Equilibrium states of generic quantum systems subject to periodic driving, *Phys. Rev. E* **90**, 012110 (2014).
- [5] M. Bukov, L. D'Alessio, and A. Polkovnikov, Universal high-frequency behavior of periodically driven systems: From dynamical stabilization to Floquet engineering, *Adv. Phys.* **64**, 139 (2015).
- [6] D. A. Abanin, W. De Roeck, and F. H. Lüscher, Exponentially slow heating in periodically driven many-body systems, *Phys. Rev. Lett.* **115**, 256803 (2015).
- [7] T. Kuwahara, T. Mori, and K. Saito, Floquet-Magnus theory and generic transient dynamics in periodically driven many-body quantum systems, *Ann. Phys.* **367**, 96 (2016).
- [8] S. A. Weidinger and M. Knap, Floquet prethermalization and regimes of heating in a periodically driven, interacting quantum system, *Sci. Rep.* **7**, 45382 (2017).
- [9] L. M. Sieberer, T. Olsacher, A. Elben, M. Heyl, P. Hauke, F. Haake, and P. Zoller, Digital quantum simulation, trotter errors, and quantum chaos of the kicked top, *npj Quantum Inf.* **5**, 78 (2019).
- [10] A. Rubio-Abadal, M. Ippoliti, S. Hollerith, D. Wei, J. Rui, S. L. Sondhi, V. Khemani, C. Gross, and I. Bloch, Floquet prethermalization in a Bose-Hubbard system, *Phys. Rev. X* **10**, 021044 (2020).
- [11] W. Hodson and C. Jarzynski, Energy diffusion and absorption in chaotic systems with rapid periodic driving, *Phys. Rev. Res.* **3**, 013219 (2021).
- [12] A. J. McRoberts, H. Zhao, R. Moessner, and M. Bukov, Prethermalization in periodically driven nonreciprocal many-body spin systems, *Phys. Rev. Res.* **5**, 043008 (2023).
- [13] W. Beatriz, C. Fleckenstein, A. Pillai, E. de Leon Sanchez, A. Akkiraju, J. Diaz Alcala, S. Conti, P. Reshetikhin, E. Druga, M. Bukov *et al.*, Critical prethermal discrete time crystal created by two-frequency driving, *Nat. Phys.* **19**, 407 (2023).
- [14] W. W. Ho, T. Mori, D. A. Abanin, and E. G. Dalla Torre, Quantum and classical Floquet prethermalization, *Ann. Phys.* **454**, 169297 (2023).
- [15] S. Vajna, K. Klobas, T. Prosen, and A. Polkovnikov, Replica resummation of the Baker-Campbell-Hausdorff series, *Phys. Rev. Lett.* **120**, 200607 (2018).

- [16] C. Fleckenstein and M. Bukov, Thermalization and prethermalization in periodically kicked quantum spin chains, *Phys. Rev. B* **103**, 144307 (2021).
- [17] T. Mori, Heating rates under fast periodic driving beyond linear response, *Phys. Rev. Lett.* **128**, 050604 (2022).
- [18] T. Mori, Floquet prethermalization in periodically driven classical spin systems, *Phys. Rev. B* **98**, 104303 (2018).
- [19] A. Haldar, R. Moessner, and A. Das, Onset of Floquet thermalization, *Phys. Rev. B* **97**, 245122 (2018).
- [20] O. Howell, P. Weinberg, D. Sels, A. Polkovnikov, and M. Bukov, Asymptotic prethermalization in periodically driven classical spin chains, *Phys. Rev. Lett.* **122**, 010602 (2019).
- [21] A. Pizzi, A. Nunnenkamp, and J. Knolle, Classical prethermal phases of matter, *Phys. Rev. Lett.* **127**, 140602 (2021).
- [22] T. N. Ikeda and A. Polkovnikov, Fermi's golden rule for heating in strongly driven Floquet systems, *Phys. Rev. B* **104**, 134308 (2021).
- [23] B. Ye, F. Machado, and N. Y. Yao, Floquet phases of matter via classical prethermalization, *Phys. Rev. Lett.* **127**, 140603 (2021).
- [24] H.-K. Jin, J. Knolle, and M. Knap, Fractionalized prethermalization in a driven quantum spin liquid, *Phys. Rev. Lett.* **130**, 226701 (2023).
- [25] N. K. Lysne, K. W. Kuper, P. M. Poggi, I. H. Deutsch, and P. S. Jessen, Small, highly accurate quantum processor for intermediate-depth quantum simulations, *Phys. Rev. Lett.* **124**, 230501 (2020).
- [26] L. K. Joshi, A. Elben, A. Vikram, B. Vermersch, V. Galitski, and P. Zoller, Probing many-body quantum chaos with quantum simulators, *Phys. Rev. X* **12**, 011018 (2022).
- [27] B. V. Chirikov, Research Concerning the Theory of Non-Linear Resonance and Stochasticity, Tech. Rep. CM-P00100691 (1971).
- [28] F. Haake, M. Kuś, and R. Scharf, Classical and quantum chaos for a kicked top, *Z. Phys. B* **65**, 381 (1987).
- [29] K. Kaneko and T. Konishi, Diffusion in hamiltonian dynamical systems with many degrees of freedom, *Phys. Rev. A* **40**, 6130 (1989).
- [30] T. Konishi and K. Kaneko, Diffusion in Hamiltonian chaos and its size dependence, *J. Phys. A: Math. Gen.* **23**, L715 (1990).
- [31] M. Falcioni, U. M. B. Marconi, and A. Vulpiani, Ergodic properties of high-dimensional symplectic maps, *Phys. Rev. A* **44**, 2263 (1991).
- [32] M. Mulansky, K. Ahnert, A. Pikovsky, and D. Shepelyansky, Strong and weak chaos in weakly nonintegrable many-body Hamiltonian systems, *J. Stat. Phys.* **145**, 1256 (2011).
- [33] B. Chirikov and V. Vecheslavov, Arnold diffusion in large systems, *J. Exp. Theor. Phys.* **85**, 616 (1997).
- [34] M. Richter, S. Lange, A. Bäcker, and R. Ketzmerick, Visualization and comparison of classical structures and quantum states of four-dimensional maps, *Phys. Rev. E* **89**, 022902 (2014).
- [35] R. Citro, E. G. Dalla Torre, L. D'Alessio, A. Polkovnikov, M. Babadi, T. Oka, and E. Demler, Dynamical stability of a many-body Kapitza pendulum, *Ann. Phys.* **360**, 694 (2015).
- [36] E. B. Rozenbaum and V. Galitski, Dynamical localization of coupled relativistic kicked rotors, *Phys. Rev. B* **95**, 064303 (2017).
- [37] S. Lellouch, A. Rançon, S. De Bièvre, D. Delande, and J. C. Garreau, Dynamics of the mean-field-interacting quantum kicked rotor, *Phys. Rev. A* **101**, 043624 (2020).
- [38] A. Kundu, A. Rajak, and T. Nag, Dynamics of fluctuation correlation in a periodically driven classical system, *Phys. Rev. B* **104**, 075161 (2021).
- [39] P. Haldar, S. Mu, B. Georgeot, J. Gong, C. Miniatura, and G. Lemarié, Rayleigh-Jeans prethermalization and wave condensation in a nonlinear disordered Floquet system, *Europhys. Lett.* **144**, 63001 (2024).
- [40] A. Russomanno, M. Fava, and R. Fazio, Chaos and subdiffusion in infinite-range coupled quantum kicked rotors, *Phys. Rev. B* **103**, 224301 (2021).
- [41] M. Martinez, P.-É. Larré, D. Delande, and N. Cherroret, Low-energy prethermal phase and crossover to thermalization in nonlinear kicked rotors, *Phys. Rev. A* **106**, 043304 (2022).
- [42] A. Cao, R. Sajjad, H. Mas, E. Q. Simmons, J. L. Tanlimco, E. Nolasco-Martinez, T. Shimasaki, H. E. Kondakci, V. Galitski, and D. M. Weld, Interaction-driven breakdown of dynamical localization in a kicked quantum gas, *Nat. Phys.* **18**, 1302 (2022).
- [43] A. Rajak, I. Dana, and E. G. Dalla Torre, Characterizations of prethermal states in periodically driven many-body systems with unbounded chaotic diffusion, *Phys. Rev. B* **100**, 100302(R) (2019).
- [44] X. Wen, R. Fan, A. Vishwanath, and Y. Gu, Periodically, quasiperiodically, and randomly driven conformal field theories, *Phys. Rev. Res.* **3**, 023044 (2021).
- [45] C. I. Timms, L. M. Sieberer, and M. H. Kolodrubetz, Quantized Floquet topology with temporal noise, *Phys. Rev. Lett.* **127**, 270601 (2021).
- [46] S. Pilatowsky-Cameo, C. B. Dag, W. W. Ho, and S. Choi, Complete hilbert-space ergodicity in quantum dynamics of generalized fibonacci drives, *Phys. Rev. Lett.* **131**, 250401 (2023).
- [47] A. Verdeny, J. Puig, and F. Mintert, Quasi-periodically driven quantum systems, *Z. Naturforsch. A* **71**, 897 (2016).
- [48] P. T. Dumitrescu, R. Vasseur, and A. C. Potter, Logarithmically slow relaxation in quasiperiodically driven random spin chains, *Phys. Rev. Lett.* **120**, 070602 (2018).
- [49] B. Mukherjee, A. Sen, D. Sen, and K. Sengupta, Restoring coherence via aperiodic drives in a many-body quantum system, *Phys. Rev. B* **102**, 014301 (2020).
- [50] B. Lapiere, K. Choo, A. Tiwari, C. Tauber, T. Neupert, and R. Chitra, Fine structure of heating in a quasiperiodically driven critical quantum system, *Phys. Rev. Res.* **2**, 033461 (2020).
- [51] H. Zhao, F. Mintert, R. Moessner, and J. Knolle, Random multipolar driving: Tunably slow heating through spectral engineering, *Phys. Rev. Lett.* **126**, 040601 (2021).
- [52] Z. Cai,  $\frac{1}{3}$  power-law universality class out of stochastic driving in interacting systems, *Phys. Rev. Lett.* **128**, 050601 (2022).
- [53] C. Ying, Q. Guo, S. Li, M. Gong, X.-H. Deng, F. Chen, C. Zha, Y. Ye, C. Wang, Q. Zhu *et al.*, Floquet prethermal phase protected by U(1) symmetry on a superconducting quantum processor, *Phys. Rev. A* **105**, 012418 (2022).
- [54] G. He, B. Ye, R. Gong, Z. Liu, K. W. Murch, N. Y. Yao, and C. Zu, Quasi-Floquet prethermalization in a disordered dipolar spin ensemble in diamond, *Phys. Rev. Lett.* **131**, 130401 (2023).
- [55] D. M. Long, P. J. D. Crowley, and A. Chandran, Many-body localization with quasiperiodic driving, *Phys. Rev. B* **105**, 144204 (2022).

- [56] T. Martin, I. Martin, and K. Agarwal, Effect of quasiperiodic and random noise on many-body dynamical decoupling protocols, *Phys. Rev. B* **106**, 134306 (2022).
- [57] H. Zhao, J. Knolle, and R. Moessner, Temporal disorder in spatiotemporal order, *Phys. Rev. B* **108**, L100203 (2023).
- [58] V. Tiwari, D. S. Bhakuni, and A. Sharma, Dynamical localization and slow dynamics in quasiperiodically-driven quantum systems, [arXiv:2302.12271](https://arxiv.org/abs/2302.12271) (2023).
- [59] D. V. Else, W. W. Ho, and P. T. Dumitrescu, Long-lived interacting phases of matter protected by multiple time-translation symmetries in quasiperiodically driven systems, *Phys. Rev. X* **10**, 021032 (2020).
- [60] T. Mori, H. Zhao, F. Mintert, J. Knolle, and R. Moessner, Rigorous bounds on the heating rate in Thue-Morse quasiperiodically and randomly driven quantum many-body systems, *Phys. Rev. Lett.* **127**, 050602 (2021).
- [61] G. Casati, I. Guarneri, and D. L. Shepelyansky, Anderson transition in a one-dimensional system with three incommensurate frequencies, *Phys. Rev. Lett.* **62**, 345 (1989).
- [62] G. Lemarié, B. Grémaud, and D. Delande, Universality of the anderson transition with the quasiperiodic kicked rotor, *Europhys. Lett.* **87**, 37007 (2009).
- [63] T. Goldfriend and J. Kurchan, Quasi-integrable systems are slow to thermalize but may be good scramblers, *Phys. Rev. E* **102**, 022201 (2020).
- [64] M. Santhanam, S. Paul, and J. B. Kannan, Quantum kicked rotor and its variants: Chaos, localization and beyond, *Phys. Rep.* **956**, 1 (2022).
- [65] V. Vuatelet and A. Raçon, Dynamical many-body delocalization transition of a Tonks gas in a quasi-periodic driving potential, *Quantum* **7**, 917 (2023).
- [66] S. Nandy, A. Sen, and D. Sen, Aperiodically driven integrable systems and their emergent steady states, *Phys. Rev. X* **7**, 031034 (2017).
- [67] A. Kruscha, R. Ketzmerick, and H. Kantz, Biased diffusion inside regular islands under random symplectic perturbations, *Phys. Rev. E* **85**, 066210 (2012).
- [68] The area is given by the expression:
- $$A(Q, P) = \frac{\pi[M_{12}P^2 - M_{21}Q^2 + (M_{11} - M_{22})QP]}{\sqrt{1 - (\frac{M_{11}+M_{22}}{2})^2}},$$
- as a function of  $Q$  and  $P$ , and  $M_{ij}$  denotes the matrix elements of  $\bar{M}'$  [72].
- [69] F. Cataliotti, S. Burger, C. Fort, P. Maddaloni, F. Minardi, A. Trombettoni, A. Smerzi, and M. Inguscio, Josephson junction arrays with Bose-Einstein condensates, *Science* **293**, 843 (2001).
- [70] I. Bloch, J. Dalibard, and W. Zwerger, Many-body physics with ultracold gases, *Rev. Mod. Phys.* **80**, 885 (2008).
- [71] A. Rajak, R. Citro, and E. G. Dalla Torre, Stability and pre-thermalization in chains of classical kicked rotors, *J. Phys. A: Math. Theor.* **51**, 465001 (2018).
- [72] A. J. Lichtenberg and M. A. Leiberman, *Regular and Chaotic Dynamics* (Springer Science & Business Media, New York, 2013), Vol. 38.